South African Journal of Geomatics, Vol. 13. No. 2, July 2024

Impact of Landuse change on Urban Thermal Variance in Umuahia Urban, Nigeria: a Remote Sensing-based Approach

Ike, Felix[1] Nkemdirim Victor U[1] and Eneogwe, Innocent, C [2]
[1] Department of Geography and Planning, Abia State University, Uturu, Nigeria,
chiemzy@yahoo.com
[2]Department of Architecture Abia State University, Uturu, Nigeria

DOI: https://dx.doi.org/10.4314/sajg.v13i2.6

Abstract

Urbanization is directly related to changes in land surface temperature (LST). However, little is known about the spatial and temporal impact of urbanization on Urban Thermal Variance (UTV) in Umuahia. To this end, we quantified the spatiotemporal associations of UTV intensity between 1986 and 2017. We calculated LST change by using a land-use change map and computed the level of vegetation coverage based on the Normalized Difference Vegetation Index (NDVI), and the Urban Thermal Field Variance Index (UTFVI). In so doing, we could determine the ecological index from multi-temporal Landsat data. Results showed that, at the expense of other types of land cover, the built-up portions of the study area were progressively increasing in surface area with a concomitant increase in temperature. The transfer matrix developed in this study reveals that within the 31-year period there was a transformation of about 59.88% and 8.23% from vegetation and bareland, respectively, to built-up cover. The spatio-temporal distribution of surface temperature showed that the built-up areas recorded the highest annual mean temperatures of 21.50^{o}C in 1986, 22.20^{o}C in 2001, and 26.01^{o}C in 2017. Results of the UTFVI showed that more areas were undergoing deteriorating ecological change and imbalances, thus leading to an increase in the area affected by the strong heat island phenomenon, which accounted for 0.065% of the total study area in 1986, 1.02% in 2000, and 32.91% in 2017. We concluded that urbanization has increased the overall surface temperature of the city. However, owing to the re-location of the city's main market, there has been a decline in UTFV in the vicinity of the city centre. The research findings indicate that the implementations of effective plans to mitigate the heat island effects are imperative for the promotion of sustainable urban development.

1. Introduction

Urbanization in sub-Saharan Africa is marked by the movement of people from rural areas to cities (Al-Yasiry, Al-Lami and Al-Maliki, 2023; Hoelscher *et al.*, 2023).Urbanization in the humid tropics degrades the vegetation cover and transforms land surface dynamics to the extent that local and regional climates are modified (Lambin, Geist and Lepers, 2003, 2003; Q. Cao *et al.*, 2020). Changes in local climate as a result of urbanization may lead to variations in the local surface temperatures. In cities, temperatures may rise several degrees higher than the

temperature of the surrounding rural areas,thus resulting in the urban heat island (UHI) effect(Q. Cao *et al.*, 2020; Palafox-Juárez *et al.*, 2021).

Variations in Land Surface Temperatures (LSTs) could be used to monitor urban climates, the databases of both variables proving to be invaluable in determining the conditions necessary to sustain human life and energy use. The UTFV index is derived from surface temperature data that are used as an objective measure of the UHI effect. It is one of the UHI indices that is the most used to provide a more precise description of the surface urban heat island effect (Kafy et al., 2021, Tomlinson et al., 2011). The UTFVI is higher in areas where the surface temperatures are significantly higher than those of the surrounding rural areas (Wang et al., 2017). The notable impacts of the UTFVI include but are not limited to local winds, humidity, and air quality (Sejati et al., 2019).The analysis of urban climatic patterns by using LST profiles has been achieved through diverse approaches as evidenced by the examination of satellite images and earth observations (Liu *et al.*, 2016; J. Cao *et al.*, 2020; Ma *et al.*, 2022). Earth observations, which rely on ground assessments, depend on station-focused analyses for the exposition of the contraposition of atmospheric temperature as a value demonstrating UHI predominance (Rahman *et al.*, 2022). A number of studies conducted previously have shown significant impacts on satellite-based observation systems for retrieving LST in the spatiotemporal measures of UHIs (Kafy *et al.*, 2021; Naim and Kafy, 2021; Ullah *et al.*, 2022; Nasar-u-Minallah *et al.*, 2023).

The urbanization trends occurring in Umuahia are reflected in the recent relocation of the main commercial complex from the city centre and the erection of several administrative buildings in Umuahia. The plan to relocate the Isi-gate main market in Umuahia as a result of increased urbanization and traffic congestion commenced in 1935, during the colonial era. However, it was only in 2013, that the government of Abia state broke a 78-year-old jinx by relocating the Umuahia main market to Ubani-Ibeku and its environs.

It is worth noting that, owing to the sparse network of weather stations, continuous point surface temperature data are lacking within the study area. These datasets yield individual measurements which are not a good representation of reality. Furthermore, the spatial information relating to these landcover change-temperature relationships is lacking in the study area.

A remotely sensed LST profile provides pertinent information about surface physical properties, energy balance, and heat diffusion in landscapes (Jiménez-Muñoz and Sobrino, 2003; Deilami, Kamruzzaman and Liu, 2018; J. Cao *et al.*, 2020). Umuahia Urban is one of the areas in South-eastern Nigeria that has the potential for vast commercial and residential development. Focusing on this background, this study aims to identify the intensity of the UHI effect in Umuahia by assessing the changes in land use and land cover (LULC), LSTs, and the

UTFV indices for the years 1986, 2001, and 2017. The results of this study would be beneficial for urban planners and policymakers in their planning of a sustainable urban environment.

2. Materials and Methods

2.1. The Study Area

Umuahia (Figure 1) lies in the south-eastern portion of Nigeria, between 5^0 25'0" N and 5^0 43'30" N, and between 7^0 22'0" E and 7^0 36'0" E. The land area extends across about 385.02 km^2, and in 2022 accommodated a population of about 593920.

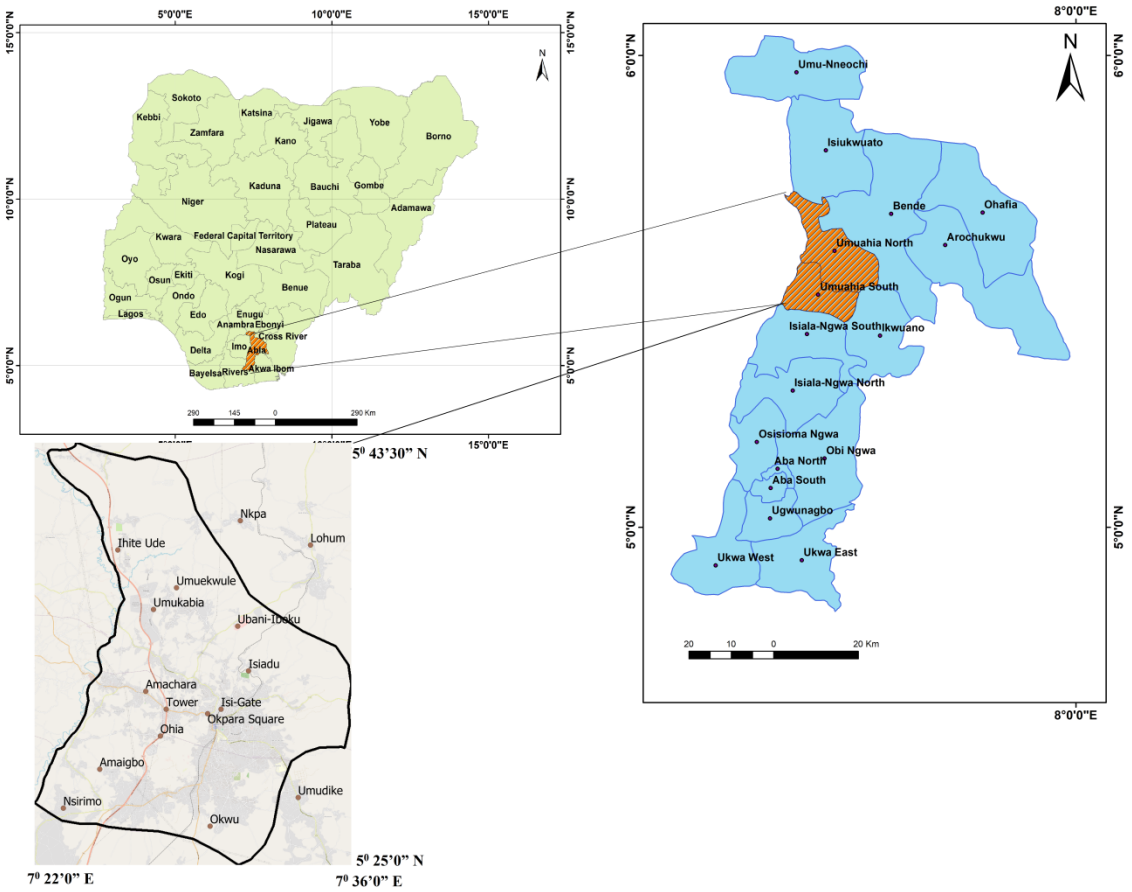

Figure 1. Location of Umuahia

The climate of the area is of the humid tropical rainforest type and is distinguished by a dry season, from November to March, and a rainy season, from April to October. The annual precipitation is approximately 2500 mm. The monthly average temperature varies from 25°C to 32°C (Ike, 2015).

2.2. Data

We used the Landsat images for the years 1986 (TM), 2001 (ETM+), and 2017 (OLI) that are freely available on the website, https://earthexplorer.usgs.gov/to extract land cover and temperature data for the study area (Refer to Table 1). We corrected the images geometrically by using 241 ground control points (GCPs) collected through the Global Positioning System (GPS) and information from the 1967 1:50 000 topographic map, that covers the study area. The selection criteria for the images were based on those used by Deilami et al. (2016). They involve three criteria: (1) a time difference of at least five years between the images, (2) similar air temperatures at the time of acquisition, and (3) cloud-free datasets.

Table 1: Sources of Satellite Data

Satellite	Sensor	Path/Row	Date	Bands	Source
LANDSAT-5	TM	056/188	12-19-1986	Digital (2-5)	USGS
LANDSAT-7	ETM+	056/188	12-21-2001	Digital (1-7)	USGS
LANDSAT-8	OLI /TIRS	056/188	12-26-2017	Digital (1-11)	USGS

3. Data analysis

3.1. Image Processing and Extraction of Surface Parameters

To retrieve surface temperature and land cover types from the image bands, the images were processed to derive the digital numbers (DN) and the top-of-atmosphere (TOA) reflectance values. The radiance values were then used to derive the underlying land cover patterns and LSTs. The Landsat TM /ETM digital numbers (DNs) were converted into TOA radiance and reflectance (P_λ)values by applying Equations 1 and 2.

$$L_\lambda = \frac{LMAX_\lambda - LMIN_\lambda}{Q_{calmax} - Q_{calmin}} \times (Q_{cal} - Q_{calmin}) + LMIN_\lambda \quad [1]$$

$$P_\lambda = \frac{(\pi \times L_\lambda \times d^2)}{(ESUN_\lambda \times \sin(\Theta)} \quad [2]$$

Where Lλ is the spectral radiance at the sensor aperture in W/ (m2sr μm); Qcal is the quantized calibrated digital number; Qcalmax and Qcalmin are the maximum and minimum quantized calibrated pixel values derived from the metadata file of the images;LMAXλ and LMINλ are the spectral radiance scales of Qcalmax and Qcalmin; d2 represents the distance between the Earth and the Sun in astronomical units; ESUNλis equivalent to the solar irradiance value; and Θ is the Sun's elevation in degrees. For Landsat OLI Data 2017, the DNs of the OLI image for the reflective 2, 3, 4, 5, 6, and 7bands and thermal band 10 were converted into TOA radiance and surface reflectance values, and based on Equations3 and 4.

$$L\lambda = MLQcal + Al \quad [3]$$

$$P\lambda = \frac{P\lambda}{\sin(\theta_{SE})} \quad [4]$$

Where Lλ is the TOA spectral radiance value, derived from the MLBand-specific multiplicative rescaling factor; Qcal represents the quantized and calibrated standard product pixel values, and Al represents the band-specific additive rescaling factor derived from the metadata; Pλ is the corrected TOA reflectance value for the Sun's angle; and θ_{SE} refers to the Sun's elevation angle, in degrees, and is derived from the metadata file associated with the OLI image.

3.2. Land Cover Classification and Accuracy Assessment

Four land cover classes were generated by means of the maximum likelihood classification method. They included built-up (amongst others, paved roads, residential and factory buildings), bare soil, water bodies, and vegetation cover A total of 100 samples were selected for each image, with 25 samples assigned to each land cover class. The data for all classes were collected from homogeneous areas during a field survey. Therefore, several factors, including the number of pixels used, the size of the dataset, the impact of spatial autocorrelation, and the differences in the images, were taken into consideration when selecting the training strategy.

3.3. Derivation of Brightness Temperature (BT) from the satellite images

Based on the method used by (Avdan and Jovanovska, 2016), the brightness temperatures derived from the TM and the OLI were estimated using thermal bands 6 and 10, respectively. Accordingly, the TOA radiance values of the thermal were converted into at-sensor brightness temperatures (B_T). The thermal constants given in the metadata file (Table 2) and Equation 5 were used for this purpose.

$$B_T = \frac{K_2}{\ln\left(\frac{K_1}{L_\lambda}+1\right)} \quad [5]$$

Where B_T is the at-sensor brightness temperature in Kelvin; $L_\lambda$is equivalent to the TOA radiance value; and K_1 and K_2 are the pre-launch calibration constants.Land Surface Emissivity (LSE) is a factor of proportionality that is used to scale the black body radiance level (Plank's law) for the purpose of measuring emitted radiance. Land surface emissivity also has the ability to transmit thermal energy across the surface into the atmosphere (Avdan& Jovanovska, 2016).

Table 2: Metadata thermal values of the images

Variable	Description	Value for Landsat 5 TM	Value for Landsat 7 ETM+	Value for Landsat 8 OLIl
K1 /K2	Thermal constants	607.76 / 1260.56	666.09/ 1282.71	774.8853/ 1321.0789
Lmax/Lmin	Maximum and Minimum values of Radiance	15.303 / 1.238	12.650/ 3.200	22.00180 / 0.10033
Qcalmax/Qcalmin	Maximum and Minimum values of Quantize Calibration	255.0/ 1.0	255.0/ 1.0	65535 / 1.0
Band	Thermal bands	Band 6	Band 6	Band 10

At the pixel scale, natural surfaces exhibit heterogeneity in terms of variation in LSE. Furthermore, LSE is significantly reliant on the surface roughness and nature of the vegetation cover (Artis and Carnahan, 1982; Richardson *et al.*, 2013). These factors can be rectified by deriving corresponding emissivity values from the Normalized Differences Vegetation Index (NDVI) values for each pixel that are based on the nature of the land cover.The emissivity level was derived by applying Equations 6a and 6b:

$$\varepsilon\lambda = \varepsilon v\lambda Pv + \varepsilon s\lambda(1 - Pv) + C\lambda \quad [6a]$$

Where ε_v and ε_s are the vegetation and soil emissivity values respectively, and C represents the surface roughness taken as a constant value of 0.005 (Jiménez-Muñoz and Sobrino, 2003).

$$P_V = \left(\frac{NDVI - NDVI_S}{NDVI_V - NDVI_S}\right)^2 \quad [6b]$$

Where P_v is the proportional vegetation cover, NDVIs is the minimum, and NDVIv is equivalent to the maximum. The generated brightness temperature values were then converted to emissivity-corrected LST values by applying Equation 7(Artis and Carnahan, 1982).

$$LST = \frac{B_T}{1+(\lambda\sigma T_B / (hc))In\varepsilon} \quad [7]$$

Where λ is the average wavelength;$\sigma$is the Boltzmann's constant (1.38×10^{-23} J/K); h is Plank's constant (6.626×10^{-34}Js); c is the velocity of light in a vacuum (2.998×10^{8} m/s); and ε is the emissivity range (between 0.991 and 0.973). Finally, the derived LSTs were converted from degrees Kelvin to degrees Celsius.

3.4. Change Detection

The methodology employed in this study involved basic image subtraction and cross tabulations to identify alterations in and conversions of the land cover and temperature pixels. Furthermore, matrices were generated to assess the qualitative and quantitative aspects of the changes in the land use classes and temperature. The software employed in this research

comprised ArcGIS 10.4, QGIS 3.1, ERDAS 9.1, and ILWIS 3.3. Additionally, Microsoft Excel 2013 was employed for the purpose of conducting analyses and creating charts and graphs.

In this study, 80 random points were selected for accuracy assessment for each image. The accuracy was checked by using a 1967 1:50 000 topographical map of Umuahia , GPS-acquired ground control points, and Google maps. The overall accuracy of the land cover maps for the years 1986, 2001, and 2017 were found to be 98%, 94%, and 98%, respectively (Table 3).

3.5. Calculation of the UTFV Index

The Urban Thermal Field Variance Index (UTFVI) for Umuahia city was calculated to quantitatively delineate the effects of urban heat islands. The UTFVI was calculated by applying Equation 8, derived from Nasar-u-Minallah *et al.*, (2023).

$$\text{UTFVI } P_V = \left(\frac{T_S - T_{mean}}{T_{mean}}\right) \quad [8]$$

Where T_S=LST, and T_{mean}= the mean temperature of the area. The UTFVI was divided into six levels by six ecological evaluation indices (Liu and Zhang, 2011).The thresholds for the six UTFV levels are presented in Table 4.

Table 3: Accuracy Assessment for the LandUse Types

Year	Classes	User accuracy (%)	Producer accuracy (%)
1986	Water	100	100
	Built-up	100	100
	Vegetation	95	95
	Bareland	90	100
	Overall Accuracy	98	
2001	Water	95	90
	Built-up	91	100
	Vegetation	100	100
	Bareland	87	85
	Overall Accuracy	94	
2017	Water	100	95
	Built-up	95	100
	Vegetation	100	100
	Bareland	87	100
	Overall Accuracy	98	

Table 4: Threshold of Ecological Evaluation Index

UTFVI	UHI phenomenon	Ecological Evaluation Index
<0	None	Excellent
0.000-0.005	Weak	Good
0.005-0.010	Middle	Normal
0.010-0.015	Strong	Bad
0.015-0.015	Stronger	Worse
>0.020	Strongest	Worst

4. Results

4.1. Spatial Pattern of Land Use/ Land Cover Change

The land cover maps produced for the years 1986, 2001, and 2017 are presented in Figure 2(a-c). In 1986, the vegetation cover occupied the greatest area in terms of spatial coverage, followed by bare land, water bodies, and built-up areas. However, by 2017, the built-up areas had expanded by 21% at the cost of the other types of land cover (Table 5).

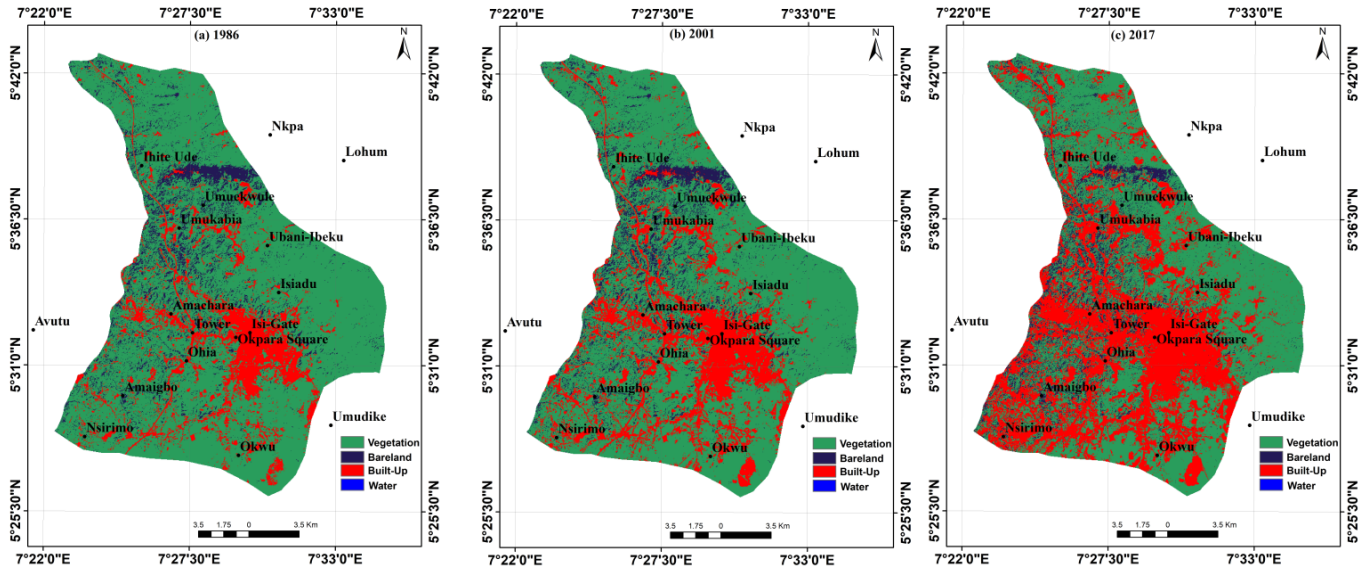

Figure 2: Changes in Land Cover for (a) 1986, (b) 2001, and (c) 2017

Table 5: Changes in Land Cover Categories

Land Cover	Total Areal Coverage in Hectares			% Change		
	1986 (%)	2001 (%)	2017 (%)	1986-2001	2001-2017	1986-2017
Bare land	4571 (11.9)	2229 (5.8)	484.76 (1.3)	-6.1	-4.5	-10.6
Built-up	2900 (7.5)	5363 (13.9)	10978 (28.5)	6.4	14.6	21
Vegetation	30905(80.3)	30805 (80.1)	26994(70.2)	-0.2	-9.9	-10.1
Water	100.49 (0.3)	80.06 (0.2)	21.37 (0.1)	-0.1	-0.1	-0.2

The transfer matrix, presented in Table 6, provides an insightful indication of various transformation probabilities, thus effectively illustrating the process of land cover transformation in a quantitative manner. The rows within the table represent the initial state (1986) of the land cover, indicating its status at that time, and the corresponding situation emanating from its transformation over time. Conversely, the columns represent the final state of the land cover, showcasing its status at that time, and the associated situation emanating from its transformation over time. It is worth noting that a significant portion of the area covered by vegetation and bare land underwent conversion into built-up land areas. Furthermore, water bodies and bare land experienced a substantial decline of approximately 10.8% in terms of their spatial coverage between 1986 and 2017. The extensive conversion of various land cover types to built-up cover, aligns with the findings of previous studies conducted by Adewole, Ike and Eludoyin (2020); Ike *et al.* (2021); Naim and Kafy (2021).

These studies highlight the increasing prevalence of built-up areas across cities in developing countries, where the extent in the area covered by the other land cover types is significantly surpassed.

Table 6: Land Cover Transformation Matrix

	Land Cover 2017					
Land Cover 1986	**CLASS**	**Built-up**	**Bare land**	**Vegetation**	**Water**	**Grand Total (ha)**
	Built-up	3453.76	173.23	732.94	0.96	4360.89
	Bare land	898.66	46.70	479.30	-	1424.67
	Vegetation	6540.46	275.08	25800.44	5.55	32621.52
	Water	29.81	0.17	40.00	1.71	71.69
	Grand Total (ha)	10922.69	495.19	27052.68	8.22	38478.77

Therefore, the transformation of areas covered by vegetation into built-up areas in Umuahia can be attributed to changes in the physical landscape, specifically in the form of rise in an increased number of administrative structures, the establishment of new settlements, and the recent relocation of certain trade centres within the study area.

4.2. LST Changes in terms of Land Cover

According to the data presented in Table 7, the average surface temperature of the study area increased by 0.43ºC between 1986 and 2001.Subsequently, a further increase of 1.92ºC was recorded between 2001 and 2017. The spatio-temporal distribution of surface temperature indicates that the built-up areas recorded the highest mean temperatures, followed by bare land, water, and vegetation cover. It is noteworthy that over the first two periods the vegetation cover exhibited considerably low radiant temperatures, possibly on account of its ability to reduce the amount of heat stored in the soil and on the surface through transpiration. The surface temperature of water, on the other hand, was generally lower than that of the other land cover classes. However, as shown in Table 8, the built-up areas experienced the highest rate of increase throughout the period.

The maximum decadal changes in surface temperature for the different types of land cover were recorded for water (1986-2001) and built-up cover/bare land (2001-2017). Correspondingly, built-up cover accounted for the maximum temperature increase for the 31year (1986-2017) period. The land cover maps reveal a significant increase in surface temperature in areas where the vegetation cover has been converted to built-up cover (Refer to Figure 3). Furthermore, observations show that, owing to the increase in built-up areas and bare surfaces, the temperature across the study area has continued to rise over time. This transformation of the respective types of land cover to built-up areas with impervious surfaces, caused by human activities, has resulted in an increase in the albedo at the surface, leading to a marginal increase in the land surface temperature around the city centre of Umuahia. Similar findings have been reported elsewhere (Kottmeier et al., 2007; Sahana et al., 2019), where natural surfaces have been found to present with lower temperatures than built-up areas.

4.3. Urban Thermal Field Variance Index

The Urban Thermal Field Variance Index (UTFVI) was used to quantitatively analyse the effects of the UHI effect on ecological degradation in Umuahia. The classification of the UTFVIs in Table 4 was employed to determine the impact (ranging from excellent to the worst case scenario) of each level. An analysis of Table 8 and Figure 4(a-c) reveals that, as opposed to the years, 1986 and 2000, in 2017, the combination of the 'no-heat-island' effect and the 'weak-heat-island' effect declined slightly around the city centre. However, the areas with moderate, strong, stronger, and strongest heat island effects remained either stable or increased between 1986 and 2017.

Table 7: Mean Land Surface Temperature

Land Cover classes	1986 Land Surface Temperature (°C)				2001 Land Surface Temperature (°C)				2017 Land Surface Temperature (°C)			
	AREA (ha)	MIN	MAX	MEAN	AREA (ha)	MIN	MAX	MEAN	AREA (ha)	MIN	MAX	MEAN
Bare land	4571	19.12	23.61	21.37	2229	19.44	23.55	21.50	484	22.61	28.00	25.31
Built-up	2900	19.10	23.90	21.50	5363	20.84	23.55	22.20	10978	23.30	28.72	26.01
Vegetation	30905	18.08	20.40	19.24	30805	15.94	22.96	19.45	26994	20.78	25.53	23.15
Water	100	19.28	20.04	19.66	80.06	19.54	22.81	21.17	21.37	21.46	22.81	22.13

Table 8: Nature of Surface Temperature Increase in Different Land Cover Classes

Class	Increase in ^{O}C from 1986-2001	Yearly increase	Decadal increase	Increase in ^{O}C from 2001-2017	Yearly increase	Decadal increase	Increase in ^{O}C from 1986-2017	Yearly increase	Decadal increase
Bare land	0.13	0.01	0.09	3.81	0.24	2.38	3.94	0.13	1.27
Built-up	0.7	0.05	0.47	3.81	0.24	2.38	4.51	0.15	1.45
Vegetation	0.21	0.01	0.14	3.7	0.23	2.31	3.91	0.13	1.26
Water	1.51	0.10	1.01	0.96	0.06	0.60	2.47	0.08	0.80

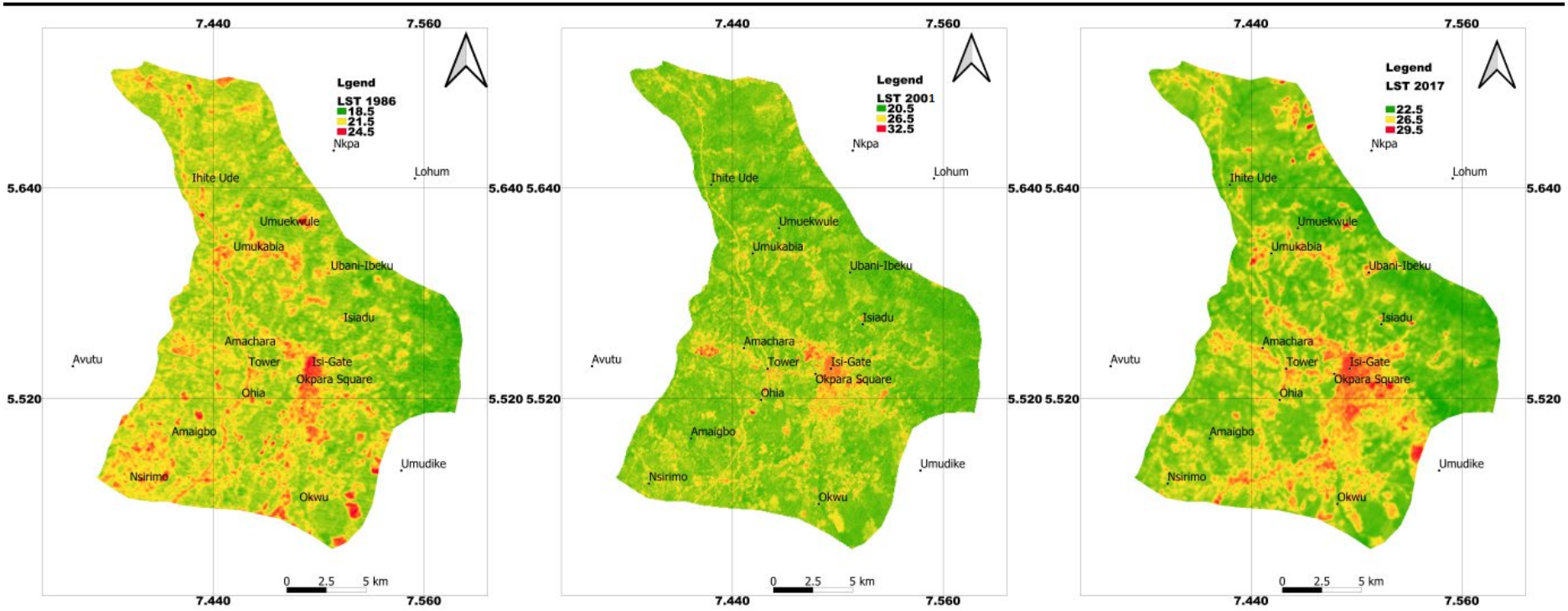

Figure 3 Land Surface Temperatures for Umuahia (a) 1986, (b) 2001, and (c) 2017

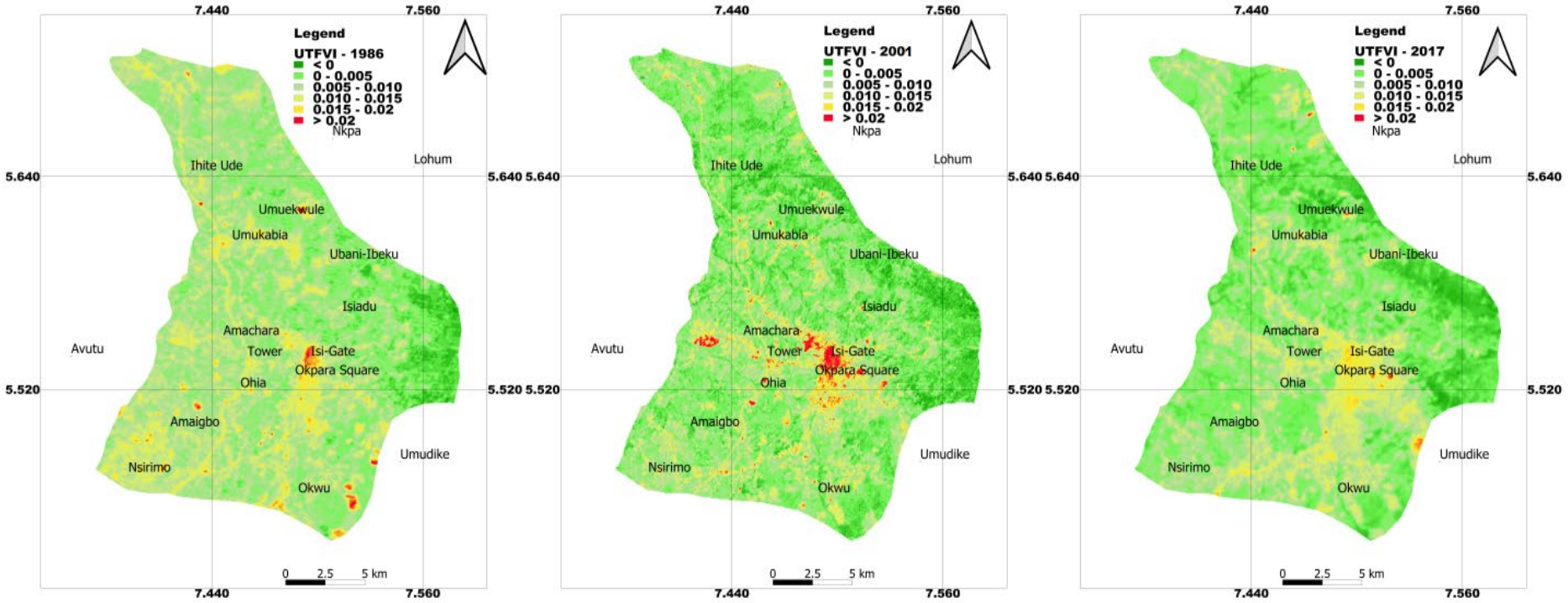

Figure 4. Urban Thermal Field Variance Indices (UTFVIs) for Umuahia

The area of 'excellent' (Refer to Table 4) heat intensity has remained constant at 58% throughout the respective study periods. However, more areas have deteriorated in terms of worsening ecological change and imbalances, thus leading to an increase in the area affected by the strong heat island phenomenon, which accounted for 0.065% of the total area researched in 1986, 1.02% of it in 2001, and 32.91% of it in 2017. This deteriorating trend in the ecological evaluation index reflects the current state of environmental degradation and the intensification of the UHI effect.

Table 8. UTFV Indices for 1986, 2001, and 2017

Threshold Values	1986(%)	2001(%)	2017(%)
<0	58%	58.81	58.755
0.000-0.005	15.69	13.86	2.32
0.005-0.010	24.05	16.15	4.61
0.010-0.015	1.5	5.1	1.25
0.015-0.02	0.065	1.02	32.91
>0.020	0.02	1.03	0.03

5. Discussion

The population of Umuahia has experienced significant exponential growth since the city attained the status of a state capital. Consequently, the city has undergone substantial expansion in its industrial and business sectors, leading to a notable transformation in land use. Prior to 1986, most of the land in Ubakala and Ohia was used primarily for agricultural purposes and for small-scale mining activities. However, after 2001, a significant portion of the land was converted into industrial and built-up land− to accommodate the rapidly increasing population. As a result, the sudden, rapid surge in population, coupled with the expansion of industrial, commercial, and residential establishments, has had a significant impact on the albedo and the land surface temperatures (LSTs) of the city. This finding concurs with the results of a study conducted by Yu *et al.*, (2019), which revealed that, compared to rural areas, urban areas have experienced a greater increase in LST. Notably, a substantial increase in temperature was observed over the built-up areas over both the analysed years. However, owing to its relocation, the densely developed Isi gate Market site exhibited a reduction in urban heat intensity between 2000 and 2017. While the heat island effect was observed predominantly over the industrial and administrative areas, the lowest LST values were experienced along the Umuekwule axis.

This increasing temperature trend identified in our study is consistent with the findings of Liu and Zhang, (2011); Deilami, and Liu, (2018); and Felix, Chiedozie and Ejimofor, (2022) which indicate that average temperatures in rapidly urbanizing regions are rising, particularly in terms of annual minimum temperatures. Overall, the urban heat island effect has been found

to be directly correlated with LST values, which are in turn influenced by land use and land cover types.

6. Conclusions

For over a century, the urban heat island effect has been a major concern all over the world. With rapid urbanization taking place in developing countries, assessments of the UHI phenomenon have become a useful tool for urban and environmental planners in monitoring and managing urban growth. It is now evident that urbanization and environmental alteration do indeed have a direct impact in that they cause increased surface temperatures in urban areas. This study, using satellite imagery and remote sensing techniques, was conducted to identify the urban heat island effect in Umuahia city that has emanated from LULC changes for the period, 1986 to 2017. Landsat TM and ETM data were used to assess LULC, NDVI, and UTFVI changes and their impacts on LSTs. The study reported drastic changes in land cover, with a corresponding increase in surface temperature for the period, 1986 to 2017, in Umuahia, south-eastern Nigeria.

Land conversion matrices also revealed a systematic conversion of vegetation into built-up cover and bare land. Correspondingly, there was a consistent decline in the area occupied by water bodies and in bare land for the period under review. Overall, built-up cover recorded the highest temperatures, followed by bare land, vegetation cover, and water bodies. The results show that urbanization has increased the overall surface temperature of the city. However, owing to the relocation of the Isi-gate Market; there has been a decline in the intensity of the urban heat island effect around the city centre.

Funding

This research did not receive any specific grant from funding agencies in the public, private and commercial, sectors.

Declaration of Competing Interests

The authors declare no conflict of interest.

Acknowledgement

The authors express their gratitude to the United States Geological Survey (USGS) for providing complimentary and easily accessible satellite images. Additionally, we extend our

appreciation to the erudite reviewers who contributed to the enhancement and finalization of this manuscript.

7. References

Adewole, A. O., Ike, F., & Eludoyin, A. O. (2019). A multi-sensor-based evaluation of the morphometric characteristics of Opa river basin in Southwest Nigeria. International Journal of Image and Data Fusion, 11(2), 185–200. https://doi.org/10.1080/19479832.2019.1683622

Al-Yasiry, A.F., Al-Lami, A.M. and Al-Maliki, A. (2023) 'Production of Environmental Sensitivity Maps for Desertification in Southern Marshes of Iraq', in *IOP Conference Series: Earth and Environmental Science*. IOP Publishing, p. 012023. Doi: 10.1088/1755-1315/1215/1/012023

Artis, D.A. and Carnahan, W.H. (1982) 'Survey of emissivity variability in thermography of urban areas', *Remote sensing of Environment*, 12(4), pp. 313–329. https://doi.org/10.1016/0034-4257(82)90043-8

Avdan, U. and Jovanovska, G. (2016) 'Algorithm for automated mapping of land surface temperature using LANDSAT 8 satellite data', *Journal of sensors*, 2016, pp. 1–8. https://doi.org/10.1155/2016/1480307

Cao, J. *et al.* (2020) 'Remote sensing inversion and spatial variation of land surface temperature over mining areas of Jixi, Heilongjiang, China', *PeerJ*, 8, p. e10257. https://doi.org/10.7717/peerj.10257

Cao, Q., Liu, Y., Georgescu, M., & Wu, J. (2020). Impacts of landscape changes on local and regional climate: a systematic review. Landscape Ecology, 35(6), 1269-1290. https://doi.org/10.1007/s10980-020-01015-7

Deilami, K., Kamruzzaman, M. and Liu, Y. (2018) 'Urban heat island effect: A systematic review of spatio-temporal factors, data, methods, and mitigation measures', *International journal of applied earth observation and geoinformation*, 67, pp. 30–42. https://doi.org/10.1016/j.jag.2017.12.009

Felix , I. ., Chiedozie , M. I. ., & Ejimofor , O. . (2022). Retrieval of Urban Land Surface Temperature Matrices from Remotely Sensed Data: An Overview. Novel Perspectives of Geography, Environment and Earth Sciences Vol. 1, 99–109. https://doi.org/10.9734/bpi/npgees/v1/2716C

Hoelscher, K., Dorward, N. M., Fox, S., Lawanson, T., Paller, J. W., & Phillips, M. L. (2023). Urbanization and political change in Africa. African affairs, 122(488), 353-376. https://doi.org/10.1093/afraf/adad021

Ike, F. (2015) 'Evaluation of the impact of climate and human induced changes on the Nigerian forest using remote sensing'. http://hdl.handle.net/10871/22127

Ike, F. *et al.* (2021) 'Effect of Land Use Changes on the Urban Surface Temperature in Umuahia Town, Southeast, Nigeria', *Nigerian Journal of Environmental Sciences and Technology (NIJEST) Vol*, 5(2), pp. 433–443.

Jiménez-Muñoz, J.C. and Sobrino, J.A. (2003) 'A generalized single-channel method for retrieving land surface temperature from remote sensing data', *Journal of Geophysical Research: Atmospheres*, 108(D22). https://doi.org/10.1029/2003JD003480

Kafy, A.-A. *et al.* (2021) 'Prediction of seasonal urban thermal field variance index using machine learning algorithms in Cumilla, Bangladesh', *Sustainable Cities and Society*, 64, p. 102542. https://doi.org/10.1016/j.scs.2020.102542

Lambin, E.F., Geist, H.J. and Lepers, E. (2003) 'Dynamics of land-use and land-cover change in tropical regions', *Annual review of environment and resources*, 28(1), pp. 205–241. https://doi.org/10.1146/annurev.energy.28.050302.105459

Liu, K. *et al.* (2016) 'Quantifying spatial–temporal pattern of urban heat island in Beijing: An improved assessment using land surface temperature (LST) time series observations from LANDSAT, MODIS, and Chinese new satellite GaoFen-1', *IEEE Journal of Selected Topics in Applied Earth Observations and Remote Sensing*, 9(5), pp. 2028–2042. doi: 10.1109/JSTARS.2015.2513598

Liu, L. and Zhang, Y. (2011) 'Urban heat island analysis using the Landsat TM data and ASTER data: A case study in Hong Kong', *Remote sensing*, 3(7), pp. 1535–1552. https://doi.org/10.3390/rs3071535

Ma, J. *et al.* (2022) 'Generating gapless land surface temperature with a high spatio-temporal resolution by fusing multi-source satellite-observed and model-simulated data', *Remote Sensing of Environment*, 278, p. 113083. https://doi.org/10.1016/j.rse.2022.113083

Naim, M.N.H. and Kafy, A.-A. (2021) 'Assessment of urban thermal field variance index and defining the relationship between land cover and surface temperature in Chattogram city: a remote sensing and statistical approach', *Environmental Challenges*, 4, p. 100107. 10.1016/j.envc.2021.100107

Nasar-u-Minallah, M. *et al.* (2023) 'Ecological monitoring of urban thermal field variance index and determining the surface urban heat island effects in Lahore, Pakistan', *Environmental Monitoring and Assessment*, 195(10), p. 1212. DOI: 10.1007/s10661-023-11799-1

Palafox-Juárez, E.B. *et al.* (2021) 'Impact of urban land-cover changes on the spatial-temporal land surface temperature in a tropical City of Mexico', *ISPRS International Journal of Geo-Information*, 10(2), p. 76. https://doi.org/10.3390/ijgi10020076

Rahman, M.N. *et al.* (2022) 'Impact of urbanization on urban heat island intensity in major districts of Bangladesh using remote sensing and geo-spatial tools', *Climate*, 10(1), p. 3. https://doi.org/10.3390/cli10010003

Richardson, A.D. *et al.* (2013) 'Climate change, phenology, and phenological control of vegetation feedbacks to the climate system', *Agricultural and Forest Meteorology*, 169, pp. 156–173. https://doi.org/10.1016/j.agrformet.2012.09.012

Ullah, N. *et al.* (2022) 'Spatiotemporal Impact of Urbanization on Urban Heat Island and Urban Thermal Field Variance Index of Tianjin City, China', *Buildings*, 12(4), p. 399. https://doi.org/10.3390/buildings12040399

Yu, Z. *et al.* (2019) 'Spatiotemporal patterns and characteristics of remotely sensed region heat islands during the rapid urbanization (1995–2015) of Southern China', *Science of the Total Environment*, 674, pp. 242–254. https://doi.org/10.1016/j.scitotenv.2019.04.088